3
Nuclear interactions

In the preceding chapter we discussed the electromagnetic interaction, which was responsible for the energy loss and small angle scattering of charged particles, and for the production and interactions of photons. However, there are other types of processes where the nuclear interaction may represent the dominant mechanism. These include particle creation reactions, interactions at high energies or large momentum transfers, and interactions of neutral particles other than the photon. In this chapter we will examine some of the basic properties of nuclear interactions. We will not be directly concerned with the physics underlying subnuclear phenomena. Instead, our main concern will be to survey its overall features, principally total cross sections, particle production multiplicities, and angular distributions.

We will first discuss the strong interaction. The group of particles known as hadrons is influenced by this interaction. Next we will briefly discuss the weak interaction, which is responsible for the interactions of neutrinos in matter and for the decay of most quasistable particles.

3.1 Strong interactions

The group of particles known as hadrons are subject to the strong interaction in matter. The neutron is an ideal probe of this interaction since it has no appreciable electromagnetic interactions. We have seen that the cross sections for most electromagnetic interactions are strongly peaked in the forward direction and fall off with increasing energy. Thus, away from the forward direction, the high energy behavior of all hadrons is determined by the strong interaction. In this section we will examine a few important features of strong interactions [1].

The total cross sections for interactions of some common hadrons on a

proton target are shown in Fig. 3.1. Most of the total cross sections have a complicated structure at low energies, due in part to resonance production. However, above 5 GeV/c incident lab momentum, the exhibited cross sections show a broad minimum where the value of the total cross section is 20–40 mb. At very high energies all the cross sections are observed to rise slowly [2]. The pp data in Fig. 3.1 show that the increase is consistent with a $\ln(s)$ dependence, where s is the square of the total CM energy. Elastic scattering represents 15–20% of the pp total cross section at high energy. Note that the negative variety of each particle has a slightly larger cross section than its positive partner. Figure 3.2 shows that similar behavior is observed in scattering from neutrons. This data is either obtained using a neutron beam or extracted from deuterium target experiments.

The rate of particle interactions I is related to the total cross section σ_T and to the incident beam rate I_0 by

$$I = I_0\left(\frac{\rho N_A t}{A}\right)\sigma_T \tag{3.1}$$

Figure 3.1 Total cross section for πp, Kp, and pp interactions as a function of the total CM energy squared, s. (After G. Giacomelli, Phys. Rep. 23: 123, 1976.)

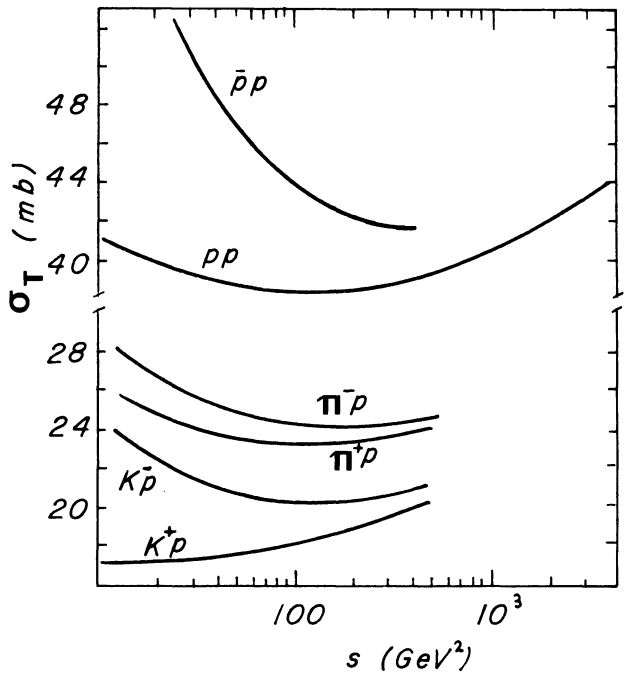

where ρ, t, and A are the density, thickness, and atomic weight of the target material. Another measure of the likelihood of an interaction is given by the mean free path between collisions (collision length)

$$L_{\text{coll}} = \frac{A}{N_A \rho \sigma_T} \tag{3.2}$$

or

$$X_{\text{coll}} = \frac{A}{N_A \sigma_T} \tag{3.3}$$

For calculations of attenuation in matter, a more relevant quantity is the absorption cross section, defined as

$$\sigma_{\text{abs}} = \sigma_T - \sigma_{\text{el}} - \sigma_q \tag{3.4}$$

where σ_{el} refers to coherent elastic scattering off a whole nucleus, and σ_q refers to quasielastic scattering from individual nucleons. In elastic and quasielastic scattering the hadron retains its identity, and its momentum is in general only slightly perturbed. We may define the absorption lengths λ of particles analogously to Eqs. 3.2 and 3.3 by replacing the total cross

Figure 3.2 Total cross section for Kn, pn, and np interactions as a function of s. (After G. Giacomelli, Phys. Rep. 23: 123, 1976.)

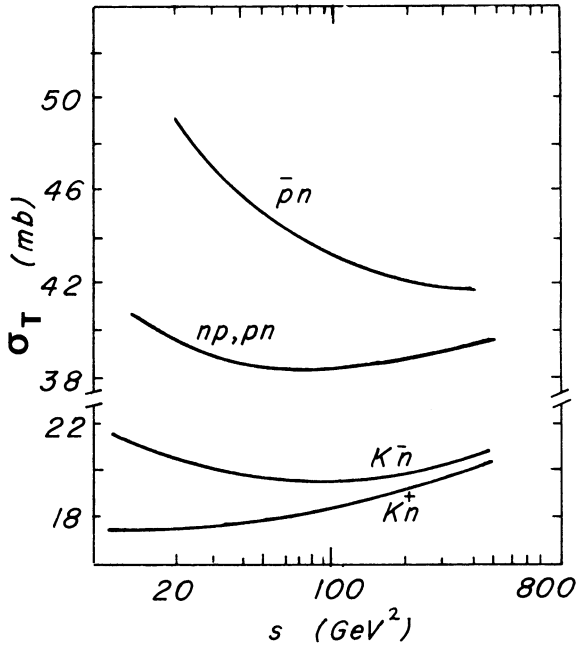

section with the absorption cross section, for example,

$$\lambda = \frac{A}{N_A \sigma_{abs}} \tag{3.5}$$

Measurements of the absorption cross section of charged hadrons from 60 to 200 GeV/c have been made by Carroll et al. [3]. The total cross section is corrected for Coulomb scattering, coherent scattering from the whole nucleus, and quasielastic scattering. The absorption cross sections are approximately independent of momentum above 20 GeV/c. Antiprotons have the largest absorption cross sections, followed in order by protons, pions, K^-, and K^+.

High energy measurements of neutron–nucleus absorption cross sections have been made by Roberts et al. [4]. Figure 3.3 shows the absorp-

Figure 3.3 Neutron–nucleus absorption (σ_I) and total (σ_T) cross sections as a function of atomic weight. (T. Roberts, H. Gustafson, L. Jones, M. Longo, and M. Whalley, Nuc. Phys. B 159: 56, 1979.)

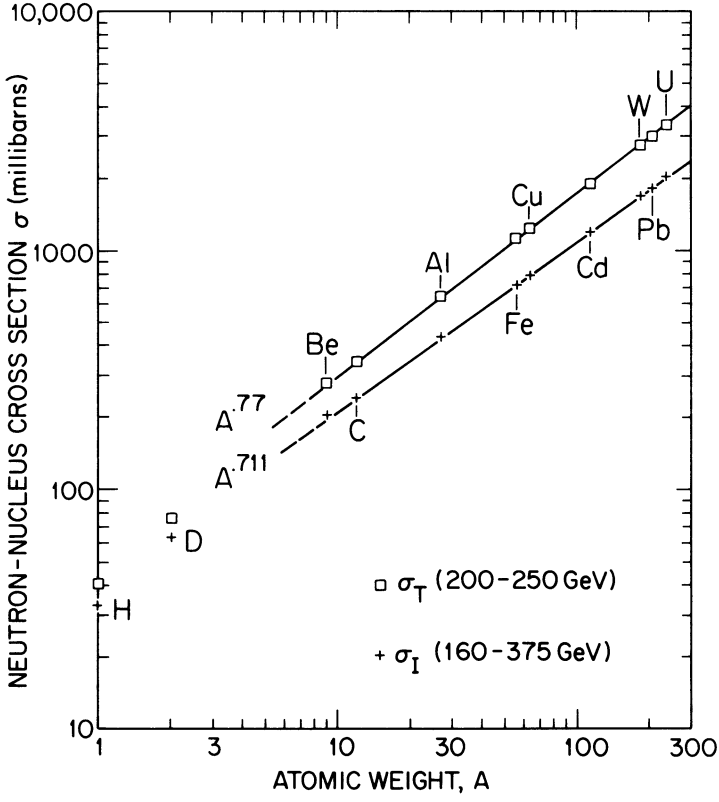

tion cross section as a function of the atomic weight of the target nucleus. It can be seen that for $A \geqslant 9$ the relation of the cross section to A is consistent with

$$\sigma_{\text{abs}}(A) = \sigma_0 A^{\alpha} \tag{3.6}$$

The fitted values of the parameters are $\sigma_0 = 41.2$ mb and $\alpha = 0.711$.

Values for nuclear collision and absorption lengths of elements are given in Table 3.1. The total cross sections refer to measurements using 80–240-GeV neutrons. Table 3.2 contains electromagnetic and nuclear properties of some common materials used in particle physics experiments.

A simple model of the nucleus indicates that $\alpha \simeq \frac{2}{3}$. Assume that the density of nuclear matter is approximately constant for all nuclei. Then the volume of the nucleus is proportional to A, the atomic weight. Assume further that the nucleons are confined in a spherical region of radius r_n. Then

$$r_n = r_0 A^{1/3} \tag{3.7}$$

where r_0 is a constant. Experimental investigations of nuclear sizes show that $r_0 = 1.38 \times 10^{-13}$ cm. Note that the experimental value for $r_0 \simeq \frac{1}{2} r_e$,

Table 3.1. *Atomic and nuclear properties of elements*

Material	Z	A	ρ^a (g/cm^3)	σ_T (barns)	X_{coll} (g/cm^2)	σ_{abs} (barns)	λ (g/cm^2)
H_2	1	1.008	0.0708	0.0387	43.3	0.033	50.8
D_2	1	2.01	0.162	0.073	45.7	0.061	53.7
He	2	4.00	0.125	0.133	49.9	0.102	65.1
Li	3	6.94	0.534	0.211	54.6	0.157	73.4
Be	4	9.01	1.848	0.268	55.8	0.199	75.2
C	6	12.01	2.265	0.331	60.2	0.231	86.3
N_2	7	14.01	0.808	0.379	61.4	0.265	87.8
O_2	8	16.00	1.14	0.420	63.2	0.292	91.0
Ne	10	20.18	1.207	0.507	66.1	0.347	96.6
Al	13	26.98	2.70	0.634	70.6	0.421	106.4
Ar	18	39.95	1.40	0.868	76.4	0.566	117.2
Fe	26	55.85	7.87	1.120	82.8	0.703	131.9
Cu	29	63.54	8.96	1.232	85.6	0.782	134.9
Sn	50	118.69	7.31	1.967	100.2	1.21	163
W	74	183.85	19.3	2.767	110.3	1.65	185
Pb	82	207.19	11.35	2.960	116.2	1.77	194
U	92	238.03	∿18.95	3.378	117.0	1.98	199

[a] Density for solids or liquids at boiling point.
Source: Particle Data Group, Rev. Mod. Phys. 56: S1, 1984.

Table 3.2. *Properties of some common materials*

Material	ρ^a (g/cm^3)	L_{rad} (cm)	X_{rad} (g/cm^2)	X_{coll} (g/cm^2)	λ (g/cm^2)
Air	(1.29)	30420	36.66	62.0	90.0
Water	1.00	36.1	36.08	60.1	84.9
Shielding concrete	2.5	10.7	26.7	67.4	99.9
Emulsion (G5)	3.815	2.89	11.0	82.0	134
BGO	7.1	1.12	7.98	97.4	156
NaI	3.67	2.59	9.49	94.8	152
BaF_2	4.83	2.05	9.91	92.1	146
CsI	4.51	1.86	8.39	—	—
Scintillator	1.032	42.4	43.8	58.4	82.0
Lucite	1.16–1.20	≈34.4	40.55	59.2	83.6
Polyethylene	0.92–0.95	≈47.9	44.8	56.9	78.8
Mylar	1.39	28.7	39.95	60.2	85.7
Pyrex	2.23	12.7	28.3	66.2	97.6

[a] Density for solids or liquids at boiling point. Number in parentheses is for gas (gm/l; STP).
Source: Particle Data Group, Rev. Mod. Phys, 56: S1, 1984; H. Grassman, E. Lorenz, and H.-G. Moser, Nuc. Instr. Meth. 228: 323, 1985.

Figure 3.4 Total cross sections for γp and γd interactions as a function of photon energy. (After G. Giacomelli, Phys. Rep. 23: 123, 1976.)

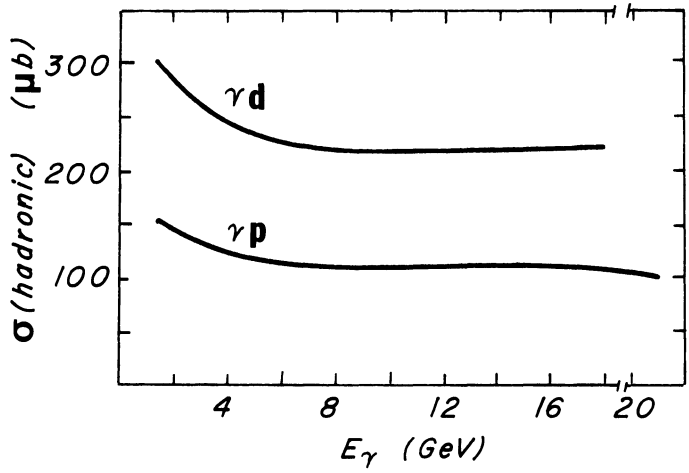

as we noted in Eq. 2.80. The geometric cross section for a point object to scatter from the nucleus is the circular area subtended by the sphere, πr_n^2, so that

$$\sigma = \pi r_0^2 A^{2/3} \tag{3.8}$$

Thus, nuclear cross sections should grow like $A^{2/3}$.

In Fig. 3.4 we show the total cross section for γp interactions. Even though the photon is not a hadron, it is believed to exist a small fraction of the time in the form of vector (spin 1) mesons. As such it exhibits behavior similar to the other hadrons. Note that the magnitude of the photoabsorption cross section is about a factor of 100 smaller than the data in Figs. 3.1 and 3.2.

The e^+e^- or e-nucleon initial state can also couple to a hadronic final state through intermediate virtual photons [5]. This is studied using the ratio R of the cross section for hadron production in e^+e^- interactions to the cross section for $\mu^+\mu^-$ production as a function of the total CM energy. Apart from particular energies, corresponding to the masses of resonance states, R is approximately 4.0 above 5 GeV. The muon pair production cross section is calculable in QED and is given in lowest order by [6]

$$\begin{aligned}\sigma_{\mu\mu} &= 4\pi\alpha^2/3s \\ &= 87.6/s \qquad \text{nb}\end{aligned} \tag{3.9}$$

where s is in GeV^2. Thus, the e^+e^- hadronic production cross section falls off like s^{-1}.

The average number of particles produced in an interaction increases as the incident energy increases [7, 8]. The top curve in Fig. 3.5 shows the average number of charged particles produced in proton–proton interactions as a function of s. We see that pp interactions with s around 1000 GeV^2 typically produce 10 charged particles. The energy dependence of the multiplicity is similar for the nonannihilation reactions in $\pi^\pm$p, $K^\pm$p, and pp. The total cross section for these interactions contains a contribution from diffractive processes. Antiproton annihilation interactions tend to produce slightly more charged particles, particularly at low energies. The differences between the two classes of interactions can be reduced if the data is plotted as a function of the energy available for particle production. This is W for $\bar{p}p$ annihilation and $W - M$ for nonannihilation reactions, where M is the total mass of the initial state particles. The average charged particle multiplicity is well fit with the equation [1]

$$\langle N \rangle = 1.8 \ln(s) - 2.8 \tag{3.10}$$

for pp interactions up to $s = 3000\ \text{GeV}^2$.

The composition of the produced particles for pp interactions is also shown in Fig. 3.5. Pions comprise about 90% of the produced particles at small angles and high energy. The fraction of charged kaons and protons tends to increase in large p_T events. Figure 3.6 shows the cross sections for inclusive production of π^0, K^0, and Λ. The measured π^0 cross sections are very close to those of π^+ and π^-. The cross sections for inclusive K^0 or Λ production are about a factor of 20 smaller at the same momentum.

Figure 3.5 Averaged charged multiplicity and charged particle composition in pp inclusive interactions. (H. Boggild and T. Ferbel, reproduced with permission, from the Annual Review of Nuclear Science, Vol. 24, © 1974 by Annual Reviews, Inc.)

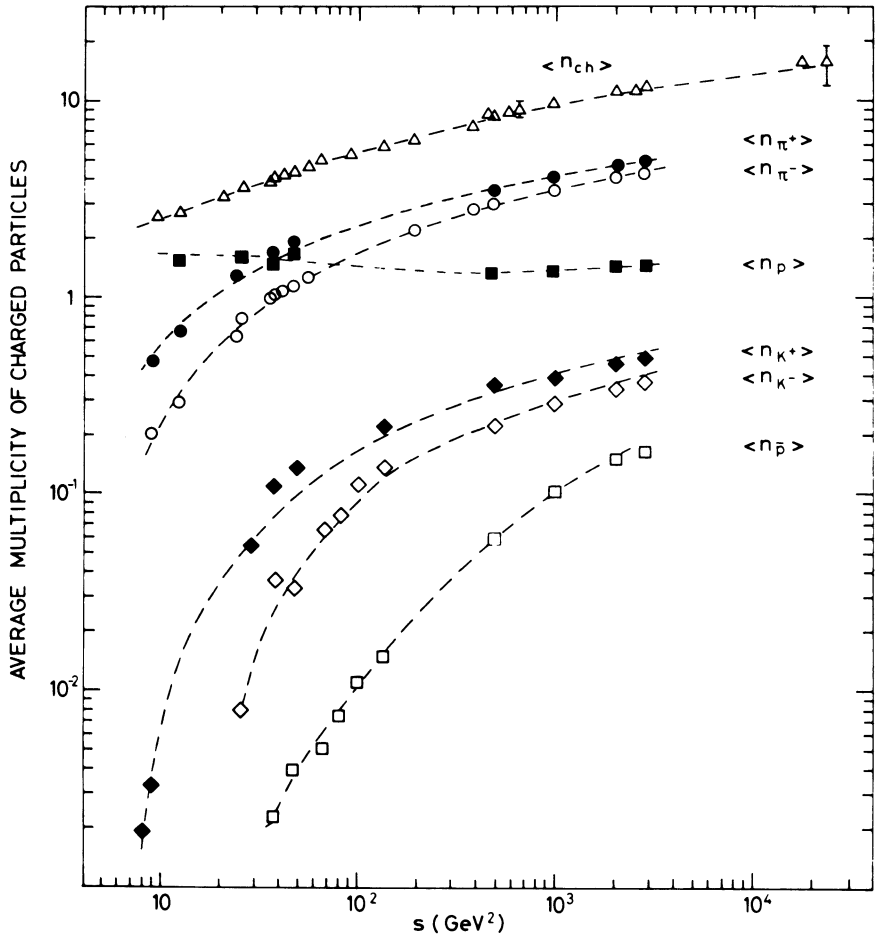

The mean charged particle multiplicity in e^+e^- interactions is similar to that observed in pp and $\bar{p}p$ interactions below $W = 5$ GeV. Above 10 GeV the muliplicity increases faster than $\ln(s)$. Particles produced with low momentum are almost entirely pions. However at $W = 30$ GeV the measured pion fraction is only around 50% for particles with momenta ≥ 4 GeV/c [5].

The angular distribution of the produced particles is mostly confined to a narrow cone around the beam direction in the laboratory. The distribution of particles is nonisotropic, even when viewed in the CM coordinate system [1]. In general, there is a particle or group of particles that is

Figure 3.6 Inclusive cross sections for the production of π^0, K^0, and Λ in pp interactions. (H. Boggild and T. Ferbel, reproduced with permission, from the Annual Review of Nuclear Science, Vol. 24, © 1974 by Annual Reviews, Inc.)

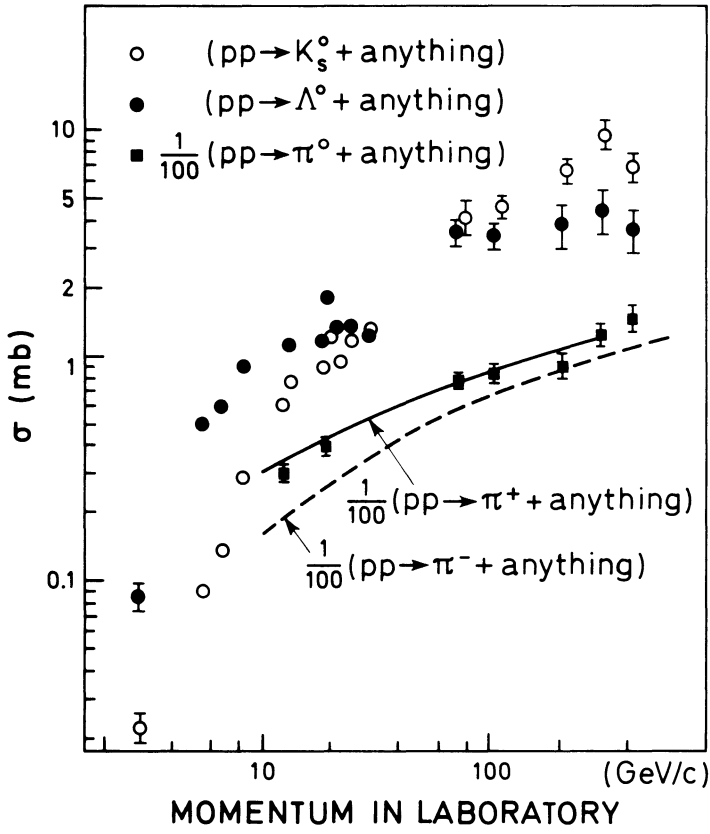

emitted at a small angle with respect to the incoming CM particles and whose momentum is larger than the other produced particles. This is referred to as the leading particle effect.

A typical pion is produced with about 300 MeV/c of transverse momentum. The transverse momentum of charged kaons or antiprotons is higher, typically ~400 MeV/c. This number grows slowly with energy. The transverse momentum distribution falls exponentially for small p_T. The invariant cross section for inclusive π^+, π^-, and π^0 production show almost identical behavior as a function of p_T. The fall-off of the cross section at large p_T is much slower than the extrapolation of the low p_T exponential, particularly at high energy [9]. The production of large p_T hadrons in e^+e^- interactions is also much larger than predicted by an extrapolation of a low p_T exponential or power law dependence [5].

3.2 Weak interactions

The second fundamental nuclear interaction is the weak interaction, which is particularly important for neutrino interactions and for the decay of most quasistable particles. Since they are neutral and not hadronic, neutrinos can act as direct probes of the weak interaction [10, 11]. The price we must pay for this good fortune is, however, that the probability of a neutrino interaction in matter will therefore be very small. This makes it more difficult to detect neutrinos than other particles.

The weak interaction sometimes plays an important role in the interactions of charged leptons. Unlike the electromagnetic and strong interactions, the weak interaction does not preserve the parity (or mirror image) symmetry. Thus, the experimental signature that allows the weak interaction effects to be separated from the electromagnetic effects is a parity-violating component in the cross section. Two important examples of this are the asymmetry measured in the scattering of polarized electrons off nuclei at SLAC [12] and the asymmetry in muon pair production in e^+e^- collisions at PETRA [5].

Two major classes of weak interactions are known. Consider for example the interaction of a ν_e with a nucleon. Weak interactions conserve the value of an internal quantum number known as the electron lepton number. In a charged current neutrino interaction the final state lepton is charged, and in this example, in order to conserve electron lepton number, it must be an electron. The interaction is believed to proceed through the exchange of a virtual W charged vector boson between the neutrino and the nucleon. In a neutral current interaction, on the other hand, the

final state lepton is neutral and in our example must be another ν_e. This interaction is believed to take place by the exchange of a virtual Z^0 neutral vector boson.

The total cross sections for ν and $\bar{\nu}$ on nucleons are shown in Fig. 3.7. It can be seen that at a given incident energy, the neutrino total cross section is about 2 times larger than the antineutrino total cross section. Both cross sections rise linearly with E_ν up to the highest energies yet measured. Notice, however, that the magnitude of the ν total cross section, even at 200 GeV, is only 160×10^{-38} cm^2, whereas a typical strong interaction cross section at the same energy is about 40 mb $= 40 \times 10^{-27}$ cm^2. The mean charged particle multiplicities for νN interactions increase like $\ln(W^2)$ above the resonance region [13].

The angular dependence is quite different for charged current ν_μN and

Figure 3.7 Total cross sections for neutrino and antineutrino interactions with nucleons as a function of the neutrino energy. (H. Fisk and F. Sciulli, reproduced with permission from the Annual Review of Nuclear and Particle Science, Vol. 32, © 1982, by Annual Reviews, Inc.)

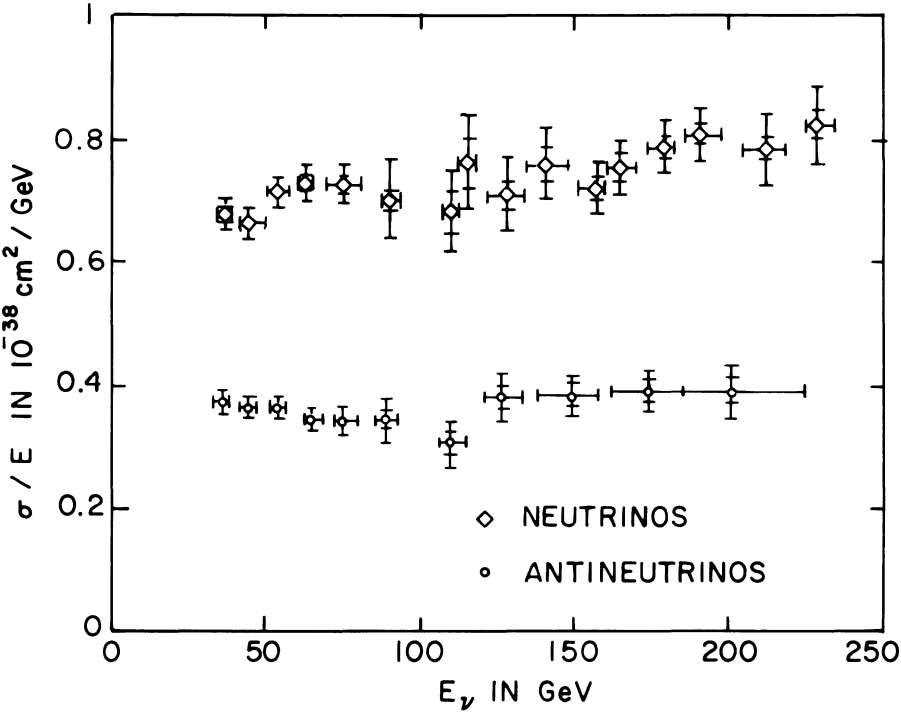

Table 3.3. *Hyperon asymmetry parameter*

Particle	Decay mode	α
Λ	$p\pi^-$	0.642 ± 0.013
	$n\pi^0$	0.646 ± 0.044
Σ^+	$p\pi^0$	-0.979 ± 0.016
	$n\pi^+$	0.068 ± 0.013
	$p\gamma$	-0.72 ± 0.29
Σ^-	$n\pi^-$	-0.068 ± 0.008
Ξ^0	$\Lambda\pi^0$	-0.413 ± 0.022
Ξ^-	$\Lambda\pi^-$	-0.434 ± 0.015
Ω^-	ΛK^-	-0.025 ± 0.028

Source: Particle Data Group, Rev. Mod. Phys. 56: S1, 1984; M. Bourquin et al., Nuc. Phys. B 241: 1, 1984.

Figure 3.8 Differential cross sections for νN and $\bar{\nu}$N scattering as a function of the variable y. (H. Fisk and F. Sciulli, reproduced with permission from the Annual Review of Nuclear and Particle Science, Vol. 32, © 1982 by Annual Reviews, Inc.)

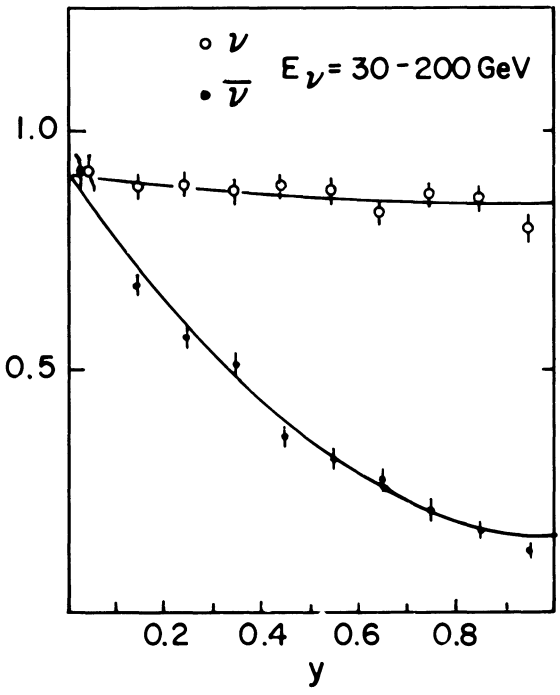

$\bar{\nu}_\mu$N scattering. Figure 3.8 shows the differential cross section plotted against the variable y, which is defined through the relation

$$1 - y = \tfrac{1}{2}(1 + \cos\theta^*) \tag{3.11}$$

where θ^* is the angle between the incident neutrino and outgoing muon in the CM system [11]. Quark–parton models predict that νN scattering should be roughly independent of y, while $\bar{\nu}$N scattering should be proportional to $(1 - y)^2$. This prediction is in good agreement with the data.

The angular distribution of the baryon in the nonleptonic decay of a spin $\frac{1}{2}$ hyperon

$$Y \rightarrow B + M$$

is given by [14]

$$I(\theta) = I_0(1 + \alpha \mathbf{P}_Y \cdot \hat{q}) \tag{3.12}$$

in the hyperon rest frame, where $\mathbf{P}_Y$ is the polarization of the decaying hyperon, $\hat{q}$ is a unit vector along the direction of the decay baryon, θ is the angle between $\mathbf{P}_Y$ and $\hat{q}$, and α is a constant associated with the particular type of decay. Table 3.3 shows measured values of α. Note that the decay distribution consists of a constant part plus a cos θ part with coefficient αP_Y. The baryons from the decay of unpolarized hyperons are produced with helicity α.

References

[1] Discussions of the theory underlying strong interactions can be found in M. Perl, *High Energy Hadron Physics,* New York: Wiley, 1974.

[2] G. Giacomelli, Total cross section and elastic scattering at high energies, Phys. Rep. 23: 123–235, 1976.

[3] A. Carroll, I.-H. Chiang, T. Kycia, K. Li, M. Marx, D. Rahm, W. Baker, D. Earty, G. Giacomelli, A. Jonckheere, P. Koehler, P. Mazur, R. Rubinstein, and O. Fackler, Absorption cross sections of $\pi^\pm$, $K^\pm$, p, and $\bar{p}$ on nuclei between 60 and 280 GeV/c, Phys. Lett. 80B: 319–22, 1979.

[4] T. Roberts, H. Gustafson, L. Jones, M. Longo, and M. Whalley, Neutron-nucleus inelastic cross sections from 160 to 375 GeV/c, Nuc. Phys. B159: 56–66, 1979. These authors use the designation σ_{inel} for the quantity that we have called σ_{abs}.

[5] P. Duinker, Review of e^+e^- physics at PETRA, Rev. Mod. Phys. 54: 325–87, 1982.

[6] P. Soding and G. Wolf, Experimental evidence on QCD, Ann. Rev. Nuc. Part. Sci. 31: 231–93, 1981.

[7] H. Boggild and T. Ferbel, Inclusive interactions, Ann. Rev. Nuc. Sci. 24: 451–513, 1974.

[8] J. Whitmore, Multiparticle production in the Fermilab bubble chambers, Phys. Rep. 27: 187–273, 1976.

[9] P. Darriulat, Large transverse momentum hadronic processes, Ann. Rev. Nuc. Part. Sci. 30: 159–210, 1980.

[10] D. Cline and W. Fry, Neutrino scattering and new particle production, Ann. Rev. Nuc. Sci. 27: 209–78, 1977.

[11] H. Fisk and F. Sciulli, Charged current neutrino interactions, Ann. Rev. Nuc. Part. Sci. 32: 499–573, 1982.
[12] E. Commins and P. Bucksbaum, The parity nonconserving electron-nucleon interaction, Ann. Rev. Nuc. Part. Sci. 30: 1–52, 1980.
[13] P. Renton and W. Williams, Hadron production in lepton-nucleon scattering, Ann. Rev. Nuc. Part. Sci. 31: 193–230, 1981.
[14] W. Williams, *An Introduction to Elementary Particles,* 2nd ed., New York: Academic Press, 1971, pp. 151–6.

Exercises

1. How many centimeters of iron would be required to reduce the intensity of a 20-GeV pion beam by 90%? How many centimeters of lead would be required?
2. What is the expected QED muon pair production cross section for the LEP 50 GeV on 50 GeV e^+e^- collider?
3. What is the expected mean charged particle multiplicity at a 20 TeV on 20-TeV proton–proton collider?
4. Do a literature search to find out how the measured $\bar{p}p$ mean charged particle multiplicity at $W = 540$ GeV agrees with the extrapolation of the pp data in Fig. 3.5.